# Increased postischemic brain injury in mice deficient in uracil-DNA glycosylase

Matthias Endres,[1] Detlev Biniszkiewicz,[2] Robert W. Sobol,[3,4] Christoph Harms,[1] Michael Ahmadi,[1] Andreas Lipski,[1] Juri Katchanov,[1] Philipp Mergenthaler,[1] Ulrich Dirnagl,[1] Samuel H. Wilson,[3] Andreas Meisel,[1] and Rudolf Jaenisch[2]

[1]Department of Neurology, Charité, Humboldt University of Berlin, Berlin, Germany. [2]Whitehead Institute for Biomedical Research, Massachusetts Institute of Technology, Cambridge, Massachusetts, USA. [3]Laboratory of Structural Biology, National Institute of Environmental Health Sciences, Research Triangle Park, North Carolina, USA. [4]Hillman Cancer Center, University of Pittsburgh Cancer Institute, Pittsburgh, Pennsylvania, USA.

**Uracil-DNA glycosylase (UNG) is involved in base excision repair of aberrant uracil residues in nuclear and mitochondrial DNA. *Ung* knockout mice generated by gene targeting are viable, fertile, and phenotypically normal and have regular mutation rates. However, when exposed to a nitric oxide donor, *Ung*$^{-/-}$ fibroblasts show an increase in the uracil/cytosine ratio in the genome and augmented cell death. After combined oxygen-glucose deprivation, *Ung*$^{-/-}$ primary cortical neurons have increased vulnerability to cell death, which is associated with early mitochondrial dysfunction. In vivo, UNG expression and activity are low in brains of naive WT mice but increase significantly after reversible middle cerebral artery occlusion and reperfusion. Moreover, major increases in infarct size are observed in *Ung*$^{-/-}$ mice compared with littermate control mice. In conclusion, our results provide compelling evidence that UNG is of major importance for tissue repair after brain ischemia.**

## Introduction

Uracil is a frequently occurring DNA base-damage residue that results from the spontaneous or chemically induced hydrolytic deamination of cytosine at a rate of approximately 100 to 500 times per cell per day (1). Uracil in DNA may also arise by misincorporation of deoxyuridine triphosphate (dUTP) opposite adenine during DNA replication. If DNA base damage is left unrepaired, it can lead to G:C to A:T transition mutations. In addition, transcriptional bypass of U:G mispairs by RNA polymerase may miscode at the lesion site and produce mutant transcripts with high efficiency (2). Hence, to protect their DNA, all known organisms express uracil-DNA glycosylases, which excise uracil residues as the first step of a base-excision repair (BER) process (1, 3, 4). In fact, greatly increased frequencies of spontaneous C:G to T:A transition mutations in mutant *E. coli* and *S. cerevisiae* that lack uracil-DNA glycosylase (*Ung* null) indicate that removal of deaminated cytosine is relevant in vivo (5, 6). In mammals, UNG function may be more redundant. A recent report indicates that the enzyme has a primary role during replication. It counteracts U:A base pairs formed by use of dUTP during DNA synthesis, while other DNA glycosylases, such as SMUG1 uracil-DNA glycosylase, may provide backup for the repair of premutagenic U:G mispairs that result from cytosine deamination in vivo (7, 8).

To characterize the biological functions of UNG, we generated knockout mice by homologous recombination. The murine *Ung* gene encodes both mitochondrial (UNG1) and nuclear (UNG2) forms of uracil-DNA glycosylase (7). The gene contains seven exons organized as are those in the human counterpart. Two alternatively spliced forms of the UNG enzyme are sorted to the nuclei (UNG2) or to the mitochondria (UNG1); the first 16 amino acids (corresponding to exon 1a) are important for mitochondrial transport. Similar to yeast, mice lacking both UNG1 and UNG2 may have a mitochondrial mutator phenotype in addition to effects on nuclear DNA (9, 10). Here, we show that *Ung*$^{-/-}$ fibroblasts and primary cortical neurons show augmented cell death when exposed to a nitric oxide donor and oxygen-glucose deprivation, respectively. Moreover, *Ung*$^{-/-}$ mice develop major increases in infarct size after focal brain ischemia compared with littermate control mice (10, 11).

## Results

*Generation of Ung*$^{-/-}$ *mice*. A targeting vector was constructed for homologous recombination to introduce a *neo* cassette so as to disrupt exons 2 to 4 in the *ung* gene and, thereby, generate a null allele (Figure 1A). This targeting vector was used to produce knockout mice by the standard blastocyst injection method. Both ES cells and mice were genotyped by Southern blotting (Figure 1B). The absence of residual UNG activity in *Ung*$^{-/-}$ cells was confirmed by activity assays (Figure 1C). Our knockout strategy left the promoter region for exon 1a intact. To determine whether residual transcription of the deleted *ung* gene occurs, we performed RT-PCR analysis. Indeed, a transcript consisting of sequences of exons 1a and 6, respectively, was detected (Figure 1D). Heterozygous *Ung*$^{+/-}$ mice appeared normal and, when interbred, yielded litters of normal size with a Mendelian genetic distribution. *Ung*$^{-/-}$ mice developed nor-

**Nonstandard abbreviations used:** anterior cerebral artery (ACA); base excision repair (BER); day(s) in vitro (DIV); deoxycytidine (dC); deoxyuridine (dU); dU triphosphate (dUTP); fluorescein diacetate (FD); lactate dehydrogenase (LDH); leukemia inhibitory factor (LIF); middle cerebral artery (MCA); MCA occlusion (MCAo); mean arterial blood pressure (MABP); mouse embryonic fibroblast (MEF); mutation frequency (MF); 3-[4-5-dimethylthiazol-2-yl]-2, 5-diphenyltetrazolium bromide (MTT); neuronal nuclei (NeuN); oxygen-glucose deprivation (OGD); phosphate buffed saline (PBS); proliferating cell nuclear antigen (PCNA); posterior communicating artery (PcomA); propidium iodide (PI); regional cerebral blood flow (rCBF); replication protein A (RPA); sodium nitroprusside (SNP); tetramethyl rhodamine ethyl ester (TMRE); thymidine kinase (TK); uracil-DNA glycosylase (UNG).

**Conflict of interest:** The authors have declared that no conflict of interest exists.

**Citation for this article:** *J. Clin. Invest.* **113**:1711–1721 (2004). doi:10.1172/JCI200420926.

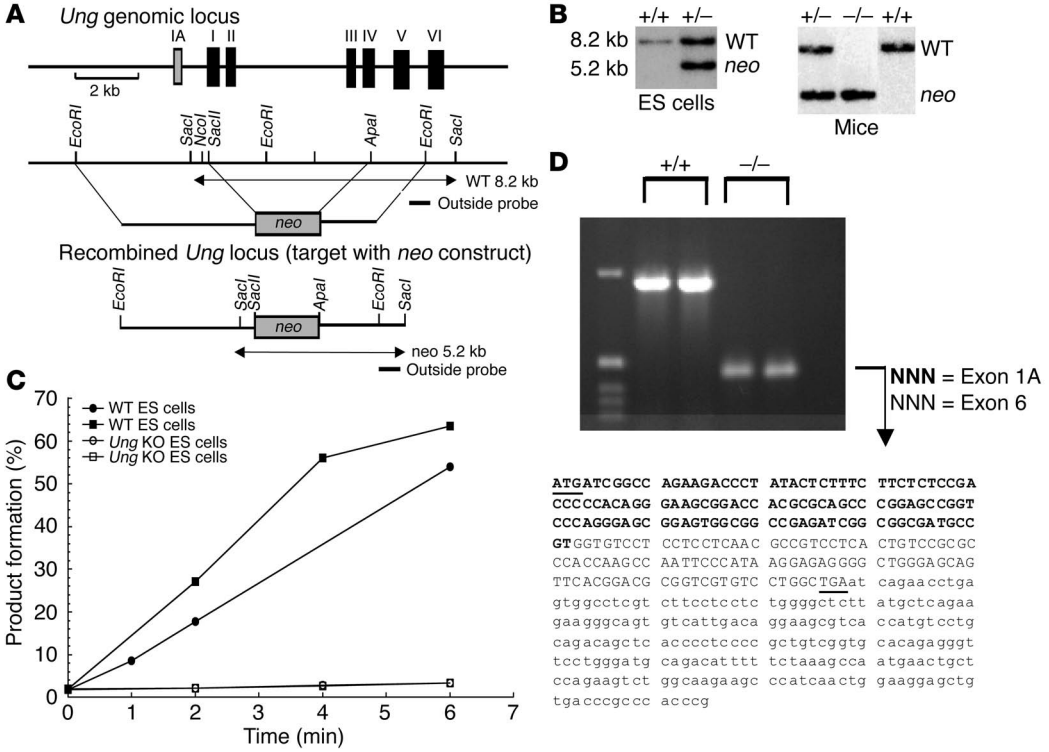


**Figure 1**
Generation of *Ung*$^{-/-}$ mice and the resulting DNA, RNA, and activity analysis. (**A**) Targeting strategy for inactivation of the *ung* gene. Lines (from top to bottom) show the map of the *ung* genomic locus, which consists of six exons (and exon 1a), the structure of the targeting construct (*neo* construct), and the resulting mutant (*neo*) allele after homologous recombination. Homologous recombination leads to the deletion of both mitochondrial (UNG1, exon 1a) and nuclear (UNG2) isoforms of uracil DNA glycosylase. Relevant Southern blot analysis was performed with the indicated 3′ outside probe. *EcoRI* digestion results in an 8.2-kb fragment in wild-type and a 5.2-kb fragment in homologus recombinations. (**B**) Exemplary Southern blot analysis of *EcoRI*-digested DNA from ES cells and mouse tissue (tails). *neo*, mutant. (**C**) Activity assays that measured the ability of *Ung*$^{+/+}$ and *Ung*$^{-/-}$ ES cell lysates to excise uracil from an end-labeled oligonucleotide substrate demonstrated no detectable enzymatic activity in the knockout cells (independent experiments). (**D**) RT-PCR in which *Ung*$^{+/+}$ and *Ung*$^{-/-}$ ES cells were used, demonstrated residual transcription of exons 1a and 6 in the recombined *ung* genomic locus. The promoter region for exon 1a was left intact by the knockout strategy and allowed residual transcription.

mally, had no overt phenotype, gained weight at a rate equal to that of wild-type mice, and had normal life spans. Moreover, they showed normal behavior, were fertile, and did not show any gross pathology on either a macroscopical or a microscopical level. Also, we observed no tendency of tumor formation up to 18 months of age (data not shown).

To determine mutation rates, we established *Ung*$^{-/-}$ mice on a homozygous Big Blue (Stratagene, La Jolla, California, USA) background and analyzed mouse embryonic fibroblasts (MEFs) for spontaneous mutant frequencies in the *cII* gene. We observed similar spontaneous mutation rates in *Ung*$^{-/-}$ compared with *Ung*$^{+/+}$ fibroblasts (Table 1).

*Increased cell death in Ung*$^{-/-}$ *fibroblasts and primary cortical neurons.* *Ung*$^{-/-}$ and *Ung*$^{+/+}$ MEF cultures were established and exposed to a nitric oxide donor, sodium nitroprusside (SNP), that has potent DNA deaminating and genotoxic effects (12). *Ung*$^{-/-}$ MEFs were significantly more vulnerable to damage and had increased cell death rates compared with *Ung*$^{+/+}$ MEFs (Figure 2A). Similar results were obtained when cells were subjected to hypoxia (<5% $O_2$) for 24 hours (40% higher cell death rates in *Ung*$^{-/-}$ compared with *Ung*$^{+/+}$ MEF at 72 hours; $P < 0.05$, Student's *t* test). To test whether enhanced susceptibility to acute oxidative stress correlated with increased uracil residues in the *Ung*$^{-/-}$ genome, we measured the ratio of deoxyuridine (dU) to deoxycytidine (dC) by reversed-phase HPLC after enzymatic hydrolysis of DNA. The dU/dC ratio was increased in untreated (naive) *Ung*$^{-/-}$ MEF compared with both *Ung*$^{+/-}$ and *Ung*$^{+/+}$ MEFs and was further enhanced by SNP exposure (Figure 2B).

To analyze the effects of *Ung* gene deletion in postmitotic differentiated cells, primary cultures of cortical neurons were established from E17 *Ung*$^{-/-}$ and *Ung*$^{+/+}$ mouse embryos. When exposed to combined oxygen and glucose-deprivation (OGD) for 120 minutes, we found that *Ung*$^{-/-}$ neurons were significantly more vulnerable to cell death than *Ung*$^{+/+}$ cells. This vulnerability was measured by fluorescein diacetate/propidium iodide staining and the release of lactate dehydrogenase (LDH) into the culture medium as a marker of cellular disruption (Figure 3, A, D, and F). In addition, there was evidence of increased mitochondrial dysfunction in *Ung*$^{-/-}$ compared with *Ung*$^{+/+}$ neurons after OGD. Reduction of 3-(4,5-dimethylthiazol-2-yl)-2,5 diphenyltetrazolium bromide (MTT) was severely compromised even at early time points in *Ung*$^{-/-}$ neurons (Figure 3B). Moreover, the loss of mitochondrial membrane potential ($\Delta\Psi_m$), which is implicated in apoptotic cascades mediated by mitochondria, was measured

**Table 1**
Mutation frequencies in *Big Blue/Ung*$^{-/-}$ and *Big Blue/Ung*$^{+/+}$ MEFs

| Number | Cell type | Total pfu | Mutants | MF (×10$^4$) | Mean |
|---|---|---|---|---|---|
| 1 | WT | 343,000 | 40 | 1.16 | |
| 2 | WT | 361,200 | 63 | 1.74 | |
| 3 | WT | 391,300 | 56 | 1.43 | |
| 4 | WT | 567,700 | 64 | 1.13 | |
| 5 | WT | 522,900 | 63 | 1.20 | |
| 6 | WT | 693,700 | 67 | 0.97 | 1.27 |
| 1 | *Ung*$^{-/-}$ | 359,800 | 51 | 1.42 | |
| 2 | *Ung*$^{-/-}$ | 810,600 | 126 | 1.55 | |
| 3 | *Ung*$^{-/-}$ | 314,300 | 49 | 1.56 | |
| 4 | *Ung*$^{-/-}$ | 333,900 | 38 | 1.14 | |
| 5 | *Ung*$^{-/-}$ | 370,300 | 74 | 1.99 | |
| 6 | *Ung*$^{-/-}$ | 321,300 | 40 | 1.24 | 1.48 |

Spontaneous mutation frequency (MF) was measured at the *cII* gene in WT and *Ung*$^{-/-}$ embryonic fibroblasts.

by tetramethyl rhodamine ethyl ester (TMRE) fluorescence. Loss of $\Delta\psi_m$ was significantly increased in *Ung*$^{-/-}$ neurons, especially at early time points (Figure 3, C and E). When neuronal cultures were exposed to milder OGD for 80 minutes, *Ung*$^{-/-}$ neurons were also significantly more vulnerable to damage, whereas susceptibility of *Ung*$^{+/-}$ neurons was not different compared with *Ung*$^{+/+}$ neurons (Table 2). Together, postmitotic *Ung*$^{-/-}$ neurons exhibited increased vulnerability to OGD, which was associated with early mitochondrial dysfunction.

*UNG expression and activity is upregulated after focal cerebral ischemia.* OGD is a common model for studying mechanisms of stroke injury in vitro. Next, we analyzed UNG expression and activity as well as the effects of *Ung* gene deletion in a model of reversible focal brain ischemia in vivo. *Ung* mRNA was detected at low levels in the brain by Northern blotting (Figure 4A). For comparison, mRNA levels were approximately 20-fold lower than in the muscle, liver, or heart and approximately fivefold lower than in the spleen or lung (Figure 4A). No full-length *Ung* mRNA transcript was expressed in cells from the *Ung*$^{-/-}$ mouse (Figure 1D), whereas mRNA for the glycosylases thymine-DNA glycosylase (TDG), alkyladenine-DNA glycosylase (AAG), and 8-oxoguanine-DNA glycosylase (OGG1) and the repair gene AP endonuclease were expressed, as determined by RT-PCR analysis (data not shown).

Mice were subjected to 30 minutes of left middle cerebral artery occlusion (MCAo) by silicone-coated, 8-0 monofilament, followed by reperfusion. After MCAo, *Ung* mRNA levels significantly increased over time in ischemic tissue of *Ung*$^{+/+}$ WT mice and peaked at 36 hours (Figure 4B). Interestingly, mRNA levels also increased in the contralateral hemisphere after MCAo (data not shown). As expected, *Ung* mRNA was not detected in the brains of *Ung*$^{-/-}$ mice (data not shown). In addition, we measured uracil-DNA glycosylase activity ex vivo in brain extracts from *Ung*$^{+/+}$ and *Ung*$^{-/-}$ mice. Because both a mitochondrial (UNG1) and a nuclear (UNG2) isoform are encoded by the *Ung* gene, we prepared both cytosolic extracts (containing mitochondria) and nuclear extracts, respectively. In the striatum of naive *Ung*$^{+/+}$ WT, mice we detected uracil-DNA glycosylase activity in the nucleus but not in the cytosolic/mitochondrial fraction (Figure 4C). After MCAo and reperfusion, there were moderate increases of nuclear uracil-DNA glycosylase activity and major increases in the cytosolic/mitochondrial fraction (Figure 4C). Similar increases were observed in brain tissue prepared from the cortex; also, there was increased activity in the contralateral hemisphere after MCAo (uracil excision per mg cytosolic protein isolated from striatum was 0% [sham], 17.9% ± 1.7% [3 h], 28.8% ± 4.4% [9 h], 16.2% ± 4.1% [24 h], 17.8% ± 3.2% [48 h], and 13.7% ± 2.4% [72 h]; $n = 3$ per time point). In sham-operated *Ung*$^{+/+}$ mice (see Methods), no activity increases were detected after 24 hours, which demonstrates that the observed effects were specific for cerebral ischemia (Figure 4C). In addition to UNG, additional enzymes in mammals have uracil-excising activity, such as SMUG1, MBD4, and TDG (1, 7). Therefore, we measured uracil-excising activity in brains from *Ung*$^{-/-}$ mice. Indeed, some activity was present in nuclear but not in cytosolic/mitochondrial extracts from both striatum and cortex of naive *Ung*$^{-/-}$ mice. Unlike in *Ung*$^{+/+}$ mice, however, activity did not increase in nuclear extracts and was still undetectable in cytosolic extracts after MCAo and reperfusion (Figure 4C).

Together, our results indicate that after MCAo and reperfusion, *Ung* mRNA and activity increase significantly. Although some of the activity detected in the nucleus may be catalyzed by enzymes other than UNG2, activity in cytosolic/mitochondrial fraction exclusively reflects UNG1 activity and is specifically and profoundly induced by ischemia and reperfusion.

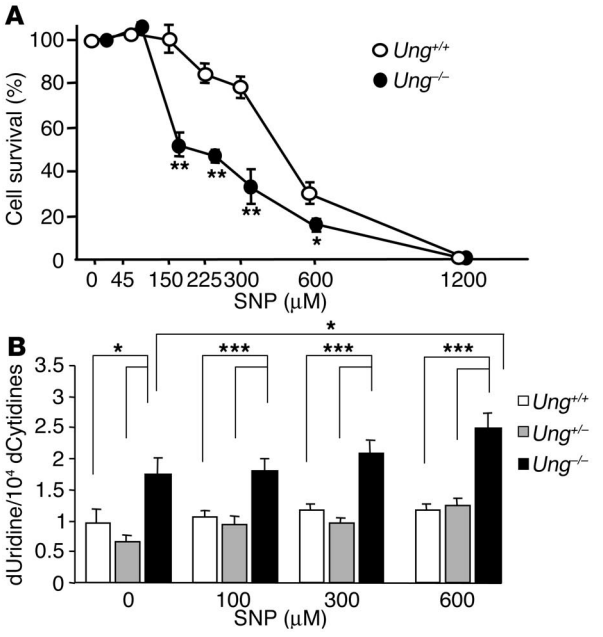


**Figure 2**
*Ung*$^{-/-}$ MEFs are susceptible to nitric oxide toxicity. (**A**) *Ung*$^{-/-}$ and *Ung* $^{+/+}$ MEF were subjected to different doses of SNP for 24 hours, which is known to induce deaminative damage. After 48 hours, viable cells were counted by trypan blue staining (mean ± SE of determinations made in three different experiments; *$P < 0.05$ and **$P < 0.01$ compared with the values in *Ung*$^{+/+}$ MEF exposed to SNP; ANOVA followed by Scheffe's post hoc test). (**B**) Increased uracil content in DNA in *Ung*$^{-/-}$ MEF after exposure to SNP. DNA was prepared from *Ung*$^{-/-}$ and *Ung*$^{+/+}$ MEF subjected to different doses of SNP, enzymatically hydrolyzed to free nucleosides, and subjected to reverse-phase HPLC. Ratios of deoxyuridine (dUridine) to deoxycytidine (dCytidine) were determined. Values are mean ± SE from three independent experiments measured in duplicate; ANOVA followed by Scheffe's post hoc test. ***$P < 0.005$.

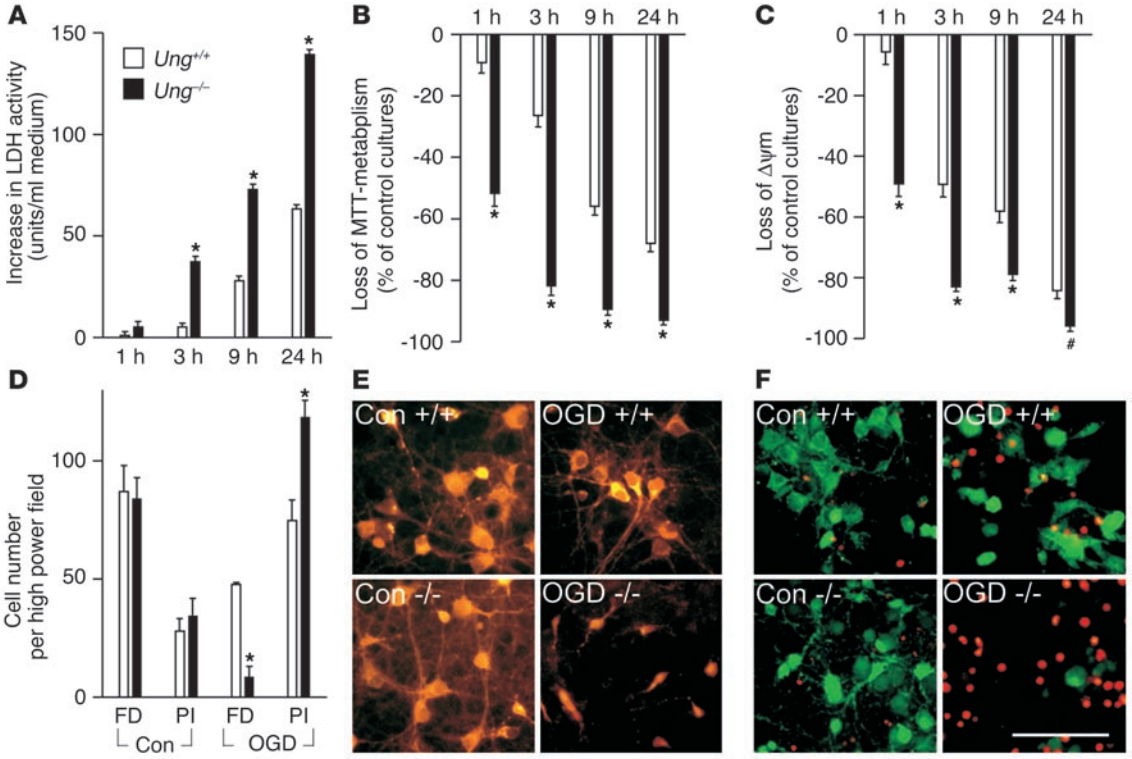


**Figure 3**
Increased cell death in Ung$^{-/-}$ neurons after oxygen-glucose deprivation. Primary cortical neurons were prepared from E17 mouse embryos. After 10 days in vitro, cells were exposed to OGD for 120 minutes. (**A**) LDH release into the culture medium was measured as a marker of cell death at different time points after OGD. Similar results were obtained with phase-contrast microscopy (not shown). (**B**) Reduction in MTT metabolism was measured 1, 3, 9, and 24 hours after OGD. (**C**) and (**E**) TMRE fluorescence measurements revealed an early and enhanced loss of mitochondrial potential ($\Delta_\psi$m) present 1 hour after reoxygenation only in *Ung*$^{-/-}$ neurons. (**D**) and (**F**) Fluorescein diacetate (FD) (green) and propidium-iodide staining (PI) (red) were used to count viable and dead cells after 24 hours. In control cultures, there were no significant differences between *Ung*$^{+/+}$ and *Ung*$^{-/-}$ neurons for basal LDH-release, MTT-metabolism, or TMRE-fluorescence. Data are mean ± SEM of two to three independent experiments. **P* < 0.001, #*P* < 0.05; ANOVA plus Tukey post hoc test. Scale bar: 50 μm.

*Tissue injury after brain ischemia is increased in Ung$^{-/-}$ mice*. To determine whether genetic deletion of *Ung* renders mice susceptible to cerebral ischemia and reperfusion, lesion size was measured by computer-assisted volumetry on hematoxylin-stained and eosin-stained coronal brain cryostat sections (20 μm) after 30 minutes of MCAo and 72 hours of reperfusion. *Ung*$^{-/-}$ mice had significantly bigger lesion volumes (>230%) than both *Ung*$^{+/+}$ and *Ung*$^{+/-}$ littermate control mice (Figure 5A). Lesions in *Ung*$^{+/-}$ mice were not statistically different from those in *Ung*$^{+/+}$ littermate control mice (Figure 5A). Significantly bigger brain lesion areas were evident in four of the five standardized coronal brain sections (2-mm distance) in *Ung*$^{-/-}$ mice (i.e., in section 2 to 5 [Figure 5B]). Although the lesioned area was confined to the striatum in *Ung*$^{+/+}$ and *Ung*$^{+/-}$ mice, it also comprised cortical tissue within the territory of the middle cerebral artery in *Ung*$^{-/-}$ mice (Figure 5C). Moreover, neuronal nuclei–positive (NeuN-positive) cells were counted within the ischemic striatum and the density of presumed viable neurons within the lesion was significantly lower in *Ung*$^{-/-}$ compared with *Ung*$^{+/+}$ mice (1,040 ± 272 cells/mm$^2$ vs. 1,328 ± 352 cells/mm$^2$; $P < 0.05$, Mann-Whitney *U* test; $n = 5$ animals and 20 visual fields per group).

Bigger cerebral lesions corresponded to worse neurologic sensory-motor deficits in *Ung*$^{-/-}$ mice compared with both *Ung*$^{+/+}$ and *Ung*$^{+/-}$ mice (Figure 5D). All animals exhibited a score of 2 or higher (i.e., moderate or severe deficit) directly after 30 minutes of MCAo. At 72 hours, however, deficits were significantly worse in *Ung*$^{-/-}$ mice compared with WT and heterozygous control mice ($P < 0.05$; Kruskall Wallis One-Way Analysis on Ranks).

Variabilities in cerebral vasculature such as the plasticity of the posterior communicating artery (PcomA) and the line of anastomoses between anterior cerebral artery (ACA) and middle cere-

**Table 2**
ΔLDH release and loss of MTT metabolism in *Ung*$^{+/+}$, *Ung*$^{+/-}$, and *Ung*$^{-/-}$ cortical neuronal cultures following 80 minutes combined oxygen-glucose deprivation

| | Δ LDH release (U/ml) | | | Loss of MTT metabolism (% of control) | | |
|---|---|---|---|---|---|---|
| Time | *Ung*$^{+/+}$ | *Ung*$^{+/-}$ | *Ung*$^{-/-}$ | *Ung*$^{+/+}$ | *Ung*$^{+/-}$ | *Ung*$^{-/-}$ |
| 1 h | 5.1 ± 2.7 | 2.7 ± 3.7 | 16.6 ± 3.8 | 12.8 ± 2.2 | 16.4 ± 3.4 | 38.7 ± 1.9$^A$ |
| 3 h | 1.6 ± 2.5 | 2.1 ± 5.5 | 28.6 ± 5.0$^A$ | 14.7 ± 4.0 | 30.0 ± 5.5$^A$ | 59.5 ± 1.9$^A$ |
| 9 h | 14.7 ± 5.6 | 8.4 ± 2.5 | 42.9 ± 3.0$^A$ | 43.7 ± 1.7 | 49.0 ± 1.9 | 71.1 ± 2.5$^A$ |
| 24 h | 27.3 ± 6.7 | 25.0 ± 4.4 | 67.4 ± 6.3$^A$ | 47.2 ± 1.1 | 45.0 ± 0.3 | 81.1 ± 3.5$^A$ |

$^A P < 0.05$ vs. *Ung*$^{+/+}$; no differences in control cultures.

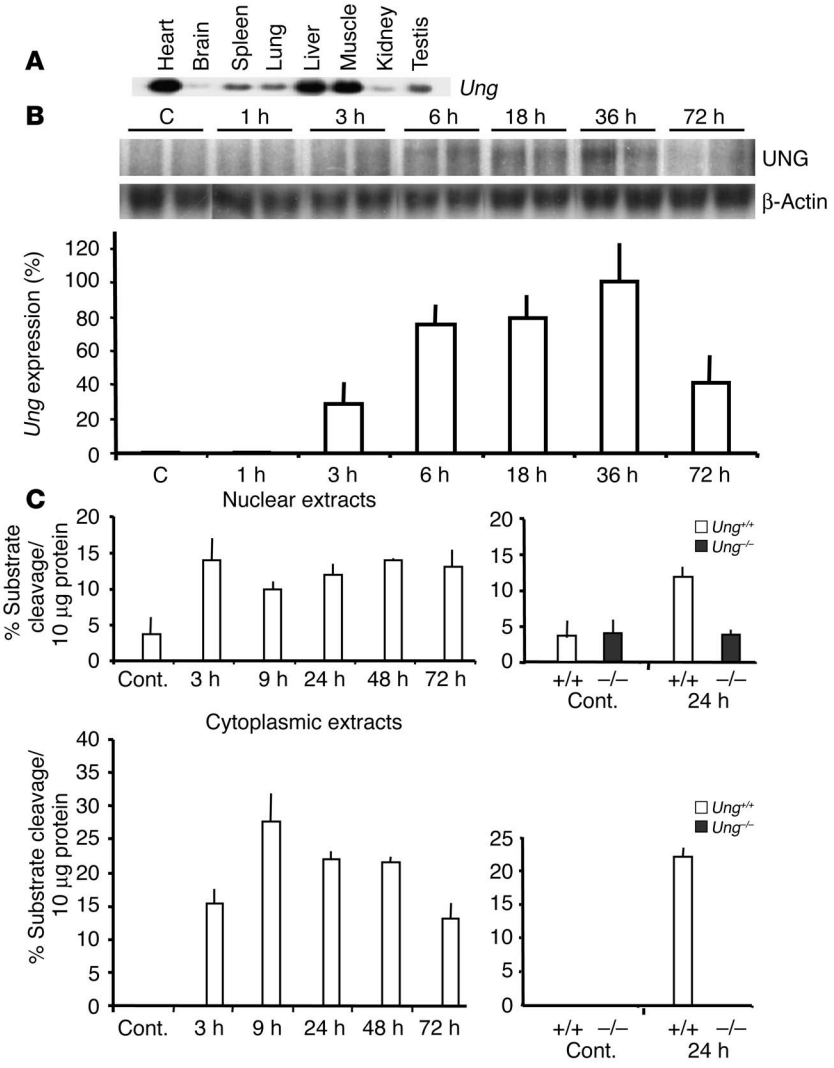


**Figure 4**
(**A** and **B**) *Ung* mRNA and (**C**) activity in different mouse tissues and in brain after filamentous MCAo. (**A**) Steady-state *Ung* mRNA expression was measured by Northern blotting according to standard techniques in several mouse organs. Expression in the brain is detectable, although at lower levels, compared with other organs. The blot is representative of three different experiments. (**B**) *Ung* mRNA after 30 minutes of MCAo was significantly upregulated over time starting at 6 hours of reperfusion with a maximum of 36 hours of reperfusion. Band intensities were quantified by densitometry and values are mean ± SEM of *Ung*/β-actin expression ratios from three independent experiments. Expression at 36 hours is set as 100%. (**C**) Uracil-DNA glycosylase activity was measured in brain extracts (nuclear and cytosolic/mitochondrial fractions, respectively) of sham-operated control mice (cont.) and at different time points after 30 minutes of MCAo.

bral artery (MCA) have been described between different mouse strains and may influence cerebral infarct size after MCAo (13, 14). To exclude possible differences between genotypes that may be caused by the mixed background, we performed carbon-black labeling in $Ung^{-/-}$ and $Ung^{+/+}$ littermate mice. No differences were observed in vascular anatomy, in development (patency) of the PcomA (Figure 5E), nor with regard to the line of MCA-ACA anastomoses (Figure 5F).

Changes in systemic physiologic parameters are known to modify outcome after cerebral ischemia. We therefore carefully monitored these parameters in randomly selected animals before, during, and after ischemia. We did not observe any significant differences in mean arterial blood pressure (MABP), blood gases (pH, partial pressure of carbon dioxide [$PaCO_2$], and arterial oxygen pressure [$PaO_2$]) or core (rectal) temperature in mutant animals compared with control animals (Table 3). In both groups, an equivalent drop in regional cerebral blood flow (rCBF) occurred at filament insertion, and an equivalent rise in rCBF occurred at filament withdrawal (Table 3). Together, it seems unlikely that changes in brain perfusion or systemic physiologic parameters contributed to the differences seen in stroke outcome.

## Discussion

We generated knockout mice to characterize the biological functions of UNG, which is implicated in the repair of aberrant uracil residues that occur as the consequence of both cytosine deamination and dUMP misincorporation during DNA replication in vivo. We found that $Ung^{-/-}$ mice had no overt phenotype and $Ung^{-/-}$ MEFs showed normal mutation rates in nuclear DNA. However, $Ung^{-/-}$ MEFs and primary cortical neurons were more susceptible to exposure to a nitric oxide donor and oxygen and glucose-deprivation, respectively, than were WT control MEFs. Moreover, $Ung^{-/-}$ mice had major increases in infarct size after focal-brain ischemia and reperfusion as compared with control littermates. Thus, UNG function seems to be redundant under baseline condition; however, it plays an important role during brain ischemia and reperfusion.

In a recent report, Nilsen et al. (7) demonstrated that mice deficient in UNG display no obvious phenotype, and they did not detect greatly increased spontaneous mutation frequencies. In their study, increased steady-state levels of up to 2,000 uracil residues were found in the *Ung* null genome, which were mostly caused by slower removal of uracil from U:A mismatch base pairs. The authors concluded that their results were at odds with a key role of UNG in the removal of uracil from premutagenic U:G mispairs

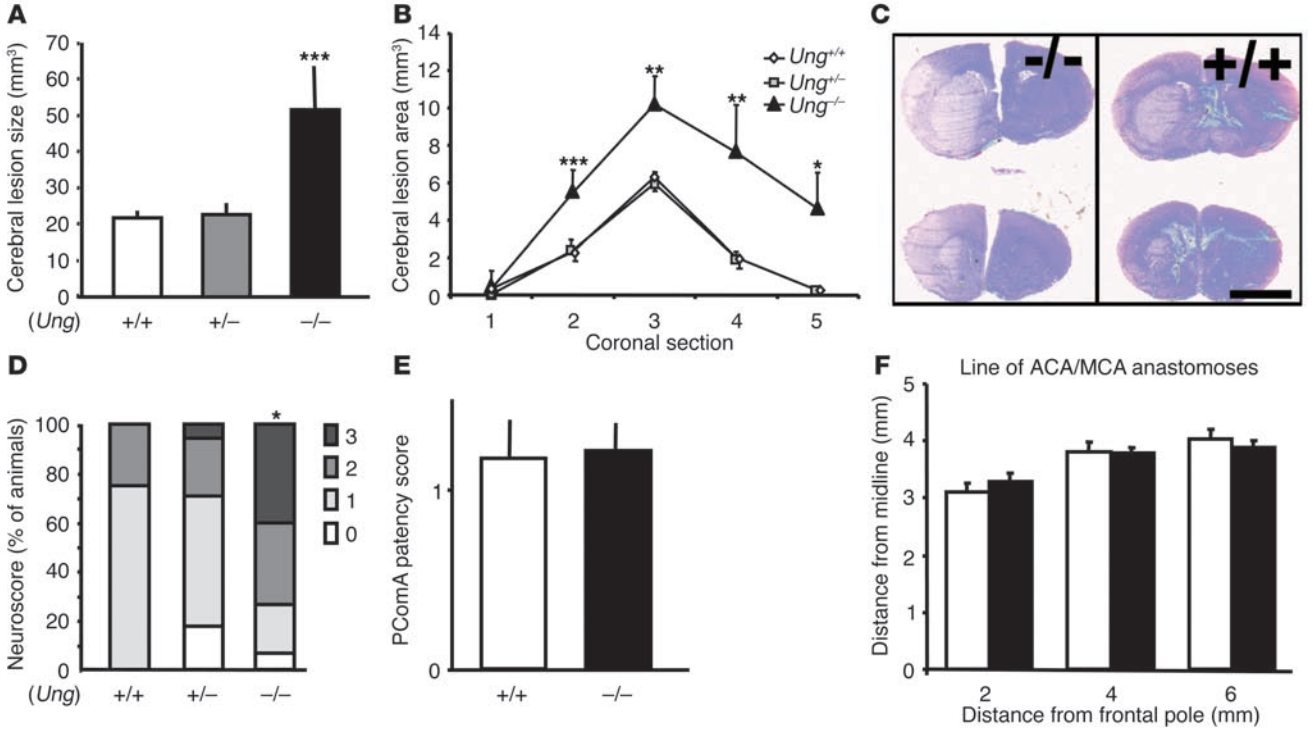


**Figure 5**

Effects of focal-brain ischemia in Ung$^{-/-}$, Ung$^{+/-}$, and Ung$^{+/+}$ littermate mice. (**A**) Brain lesion volume and (**B**) lesion areas in *Ung*$^{-/-}$ mice compared with *Ung*$^{+/-}$ and *Ung*$^{+/+}$ WT littermate mice after 30 minutes of MCAo and 72 hours of reperfusion. Brain lesion areas were determined on five anterior-posterior serial coronal H&E-stained cryostat sections (20 μm); mean ± SEM of 10 to 15 animals per group; $^{**}P < 0.01$, $^{***}P < 0.005$, ANOVA and Tukey *post hoc* test. (**C**) Typical H&E-stained 20 μm brain sections from *Ung*$^{-/-}$ and *Ung*$^{+/+}$ littermate mice. Scale bar: 3 mm. (**D**) Neurological sensory-motor deficits were determined after 72 hours and scored from 0 (no deficit) to 3 (severe); $^{*}P < 0.05$, ANOVA on ranks (Kruskall Wallis). (**E**) The development of left and right posterior communicating arteries (PcomA) was determined in carbon black–perfused brains as follows: 0, absent; 1, present but poorly developed (hypoplastic); and 2, well formed; mean ± SEM from eight animals per group; ANOVA on ranks (Kruskall Wallis). (**F**) The distance from midline of the line of anastomoses between the ACA and the MCA was determined in carbon black–perfused brains; mean ± SEM from eight animals per groups. ANOVA and Tukey post hoc test.

generated by cytosine deamination but rather have a primary role during DNA replication (7). UNG2 is predominantly colocalized with proliferating cell nuclear antigen (PCNA) and replication protein A (RPA) in replication foci (15). In addition, the mammalian repertoire of uracil-removing enzymes is larger than in bacteria, and "backup" activities from other enzymes such as MUG/TDG, SMUG1, and MBD4 may compensate for the lack of UNG (1, 16, 17). Indeed, evidence suggests that SMUG1 and not UNG has a primary role in the repair of deaminated cytosine (8).

Here, we demonstrate that *Ung*$^{-/-}$ mice show a significant phenotype after ischemic insult, which indicates that only after cell injury is the important role of UNG for DNA repair "unmasked." In fact, UNG differs from the other known uracil-excising enzymes in several ways. First, UNG is a very efficient DNA repair enzyme with a turnover number of 500 to 1000/min. Second, not only a nuclear isoform (UNG2) but also a mitochondrial isoform (UNG1) is expressed from the *Ung* gene. Third, UNG message and activity is profoundly upregulated by DNA damage (1). From our data, we propose a mitochondrial mutator phenotype in *Ung*$^{-/-}$ mice similar to findings in yeast (9).

Mice lacking UNG had major increases in cerebral infarct size and lower numbers of surviving neurons within the ischemic area after mild cerebral ischemia and reperfusion. Significantly, larger lesion areas were found in four of the five standardized coronal brain sections, and larger infarcts were accompanied by worse neurological sensory-motor scores. This finding indicates that lack of UNG also had functional consequences. Differences in neuronal densities within the ischemic lesion were modest, which indicates that a large number of neurons die after the ischemic insult, even in the presence of UNG. No differences in vascular anatomy or physiologic parameters could explain these differences on outcome. In addition, higher cell death rates were also found in *Ung*$^{-/-}$ MEFs after deaminative and oxidative damage and in postmitotic primary cortical neurons after combined oxygen-glucose deprivation. In fact, markers of mitochondrial integrity, that is, metabolism of MTT and mitochondrial membrane potential, were significantly and severely compromised in *Ung*$^{-/-}$ neurons already at early time points after injury. Interestingly, susceptibility of heterozygous *Ung*$^{+/-}$ mice to cerebral ischemia in vivo or oxygen-glucose deprivation in vitro was not different compared with WT *Ung*$^{+/+}$, which indicates that one *Ung* allele can completely compensate for the loss of the other one.

We propose that the mechanism of cell death in postmitotic neurons of UNG mutant mice after ischemic insult relates — at least in part — to the lack of UNG1 activity in mitochondria. Mitochondria are well established as a critical instigator and rein-

**Table 3**
Physiologic parameters in *Ung*$^{-/-}$ and littermate *Ung*$^{+/+}$ control mice before, during, and after MCAo

| Parameter | Ung$^{-/-}$ | Ung$^{+/+}$ |
|---|---|---|
| **MABP (mmHg)** | | |
| Before | 102 ± 6 | 101 ± 2 (NS) |
| During | 103 ± 6 | 107 ± 6 (NS) |
| After | 105 ± 6 | 106 ± 4 (NS) |
| **rCBF (%)** | | |
| Before | 100 ± 0 | 100 ± 0 (NS) |
| During | 9 ± 2 | 10 ± 2 (NS) |
| After | 80 ± 14 | 74 ± 5 (NS) |
| **pH** | | |
| Before | 7.30 ± 0.02 | 7.31 ± 0.02 (NS) |
| After | 7.34 ± 0.01 | 7.34 ± 0.04 (NS) |
| **$PaCO_2$ (mmHg)** | | |
| Before | 39.2 ± 1.3 | 35.5 ± 2.0 (NS) |
| After | 36.7 ± 3.7 | 36.5 ± 0.04 (NS) |
| **$PaO_2$ (mmHg)** | | |
| Before | 91.5 ± 8.7 | 105.1 ± 7.14 (NS) |
| After | 110.1 ± 3.7 | 105.5 ± 20.3 (NS) |
| **CT (°C)** | | |
| During | 36.8 ± 0.1 | 36.8 ± 0.1 (NS) |
| Body weight (g) | 24.7 ± 1.3 | 23.9 ± 1.0 (NS) |

Physiological parameters: MABP, arterial oxygen pressure ($pO_2$), $PaCO_2$, and pH in arterial blood samples were analyzed before, during, and after MCAo. rCBF was measured by laser-Doppler flowmetry during ischemia until 10 minutes after reperfusion and expressed as a percentage of the baseline readings. Animals were weighed before onset of the experiment. Rectal (core) temperature (CT) was kept constant by means of a feedback temperature-control unit. No statistical significant differences (NS) were found between groups ($n$ = five animals per group).

forcement site in several cell death pathways, and damage to mitochondrial genes has been linked to a number of neurologic diseases and aging (18–20). There is good evidence for base excision repair, direct damage reversal, mismatch repair, and recombinational repair mechanisms in mitochondria (21), and the presence of these enzymes in the brain has recently been confirmed (20, 22, 23). It has been suggested that insufficient mtDNA repair, and the subsequent accumulation of mutations in the mitochondrial genome, can lead to mitochondrial dysfunction and cell death (20, 24). Both, DNA damage and mitochondrial dysfunction are well-documented consequences of ischemic brain injury (10, 20). In our study, we demonstrate that *Ung* mRNA and uracil-DNA glycosylase activity were profoundly upregulated after cerebral ischemia in *Ung*$^{+/+}$ WT mice. Some uracil-DNA glycosylase activity was found in nuclear extracts from *Ung*$^{-/-}$ mice, which is most likely caused by the activity of SMUG1 (7, 8). However, the most significant increase was seen in cytosplasmic/mitochondrial extracts: uracil-DNA glycosylase activity was undetectable in nonischemic and sham-operated animals but dramatically increased after stroke. Even more importantly, no activity was detected in the cytosolic fraction of *Ung*$^{-/-}$ mice before and after ischemia and reperfusion, which confirms that uracil-DNA glycosylase activity seen in WT animals must be exclusively caused by UNG1.

Under conditions in which the repair of uracil is impaired, transcriptional base substitution at sites of uracil may be a predominant mechanism for the production of mutant proteins, especially in nondividing cells, which may account for the increased cellular vulnerability of *Ung*$^{-/-}$ mice (2). Although the pathway of cell death is delayed after 30 minutes of MCAo in vivo (25), onset of cell death is very rapid after oxygen-glucose deprivation, which would argue against a role for (mitochondrial) DNA repair as a defense against ischemia-induced cell death. However, in contrast to the in vivo data, we found that cytosolic/mitochondrial UNG activity was already elevated in unchallenged *Ung*$^{+/+}$ (but not *Ung*$^{-/-}$) neuronal cultures (not shown), which may confer increased neuronal resistance against oxygen-glucose deprivation. On the other hand, we believe it unlikely that an increase in the mutation rate of nuclear genes would contribute significantly to ischemia susceptibility in *Ung*$^{-/-}$ mice, although there remains a possibility that uracil in nuclear DNA could prove toxic (by triggering an excessive amount of mismatch repair.) In MEF, the level of alteration in the dU/dC ratio in total DNA was only modest after deaminative challenge, even though there was profound cell death in this model. Because the amount of nuclear DNA is approximately two orders of magnitude higher than that of mtDNA, damage in mtDNA may not be detected by this assay. However, we did not provide direct evidence of increased damage to mitochondrial DNA in *Ung*$^{-/-}$ neurons.

Interestingly, *Ung* expression and activity were also increased in the contralateral hemisphere after MCAo and reperfusion. In fact,

**Table 4**
Details of the RT-PCR

| Name | Product size | Forward and reverse primer sequence | Denaturation/annealing/extension conditions |
|---|---|---|---|
| TDG | 1194 bp | 5′-CAAATGATGGCAGAAGTTCCTAACATG-3′ and 5′-TTCCTAAGCGTGGCTCTCTTCTTCCTGC-3′ | 95°C, 1 min/62°C, 1 min/72°C, 2 min |
| OGG1 | 474 bp | 5′-GCTGGCAGATCAAGTATGGACACT-3′ and 5′-AGGATGGCTTTGGCACTGG-3′ | 95°C, 1 min/66°C, 0.5 min/72°C, 0.5 min |
| AAG | 374 bp | 5′-GACACCGAGCAGCCTCCATTT-3′ and 5′-CCCAAGTATGCCTCAGTCTCCACA-3′ | 95°C, 1 min/66°C, 0.5 min/72°C, 0.5 min |
| APE | 478 bp | 5′-CTTATGGCATTGGCGAGGAA-3′ and 5′-GACCGGATCTTGCTGTCACAC-3′ | 95°C, 1 min/62°C, 1 min/72°C, 1 min |
| Actin | 540 bp | 5′-GTGGGCCGCTCTAGGCACCAA-3′ and 5′-CTCTTTGATGTCACGCACGATTTC-3′ | 95°C, 1 min/60°C, 1 min/72°C, 1 min |
| UNG | 914 bp | 5′-TGCTCGGCTGGACCATGGGCGTCT-3′ and 5′-CGGGTGGGCGGGTCACAGCTCCTT-3′ | 95°C, 1 min/62°C, 1 min/72°C, 2 min |

a number of genes and gene products were found to be increased in areas remote from the ischemic lesion and in contralateral hemispheres. These genes and gene products include transcription factors, immediate early genes, heat shock proteins, respiratory chain genes, neuronal signaling, and growth factors and have been implicated in functional recovery and repair (26, 27). Induction of UNG expression and activity may be a downstream event in a systemic cascade of injury-induced responses and could be involved in the phenomenon of ischemic preconditioning (20).

In summary, we demonstrate that UNG expression and activity are induced after brain ischemia and reperfusion and that major increases in infarct volume are observed in $Ung^{-/-}$ mice. Although the exact mechanisms that contribute to increased cellular susceptibility remain to be determined, we propose that damage to mtDNA and impaired mitochondrial function are important factors.

## Methods

*Uracil-DNA glycosylase targeting construct*. We isolated an *EcoRI* restriction fragment that contained a large portion of the *ung* gene. The *EcoRI* restriction fragment was shown to contain exons 1 to 5 and the mitochondria-specific exon 1a by use of a combination of PCR and Southern hybridization techniques. The *Neo* or *hyg-tk* targeting vectors were constructed by replacing the *NcoI-ApaI* fragment with a neomycin-resistance cassette or a hygromycin-thymidine kinase–resistance cassette, thereby deleting exons 1, 2, and 3 and part of exon 4 of the *ung* gene. Homologous recombination of the *neo* targeting vector in murine 129/SvJae ES cell (J1 ES cells) resulted in the generation of $Ung^{+/neo}$ ES cells, which were used for injection in Balb/c blastocysts. To confirm homologous targeting in ES cells, isolated genomic DNAs were digested with *SacI*, separated, and blotted on Zetabind nylon membrane (CUNO, Meriden, Connecticut, USA). The blotted DNA fragments were hybridized to radioactive-labeled outside probe from exon 6. Outside probe from exon 6 was amplified from genomic DNA (5′-AAGCGTCACCATGTCCTGCAG-3′ and 5′-GAAATCTCTAACTCTAAAGGATAAAGCGG-3′). Radioactive-labeled probes were synthesized by random labeling (Prime-It-II; Stratagene). WT allele produced a band of 8.2 kb, whereas the *neo* allele and *hyg-tk* allele produce bands of 5.2 kb and 4.1 kb, respectively. Only gender-matched littermates from a mixed 129/SvJae × Balb/c background were used for experiments reported in this study.

*Cell culture and transfection*. WT ES cells (J1 ES cells) (28), $Ung^{+/-}$ mutant ES, and $Ung^{-/-}$ mutant ES cells were cultivated on irradiated MEFs as described (29) or without MEFs by use of a high concentration of leukemia inhibitory factor (LIF) (1,000 U/ml). Transfection of plasmids (*Neo* or *hyg-tk* targeting vectors) was performed by the application of the cationic liposome reagent DOTAP from Boehringer Mannheim/Roche Bioscience (Mannheim, Germany). MEFs were cultured in HEPES-buffered Dulbecco's modified Eagle medium with high glucose (Gibco-BRL, Langley, Oklahoma, USA); 10% heat-inactivated fetal calf serum (HyClone, South Logan, Utah, USA); 0.1 mM nonessential amino acids (Gibco-BRL); 0.1 mM β-mercaptoethanol (Sigma-Aldrich, Deisenhofen, Germany); LIF; and the antibiotics penicillin and streptomycin.

*Uracil-DNA glycosylase activity assay (cell culture)*. ES cells were grown without MEF. Shock-frozen cells or tissues were ground with mortar and pestle and resuspended in activity buffer (20 mM Tris-HCl, pH 7.8; 100 mM KCl; 2 mM EDTA; 1 mM EGTA; 5 mM β-mercaptoethanol; and proteinase inhibitors). Protein concentrations were normalized. Uracil excision activity in lysates was measured by the ability to excise uracil from a [γ-$^{32}$P]-ATP end-labeled oligonucleotide (5′-GCTTGCATGCCTGCAGGTCGA**U**TCTAGAGGATCCCCGGGTACCGAGCTCGA-3′) that was hybridized before to a complementary oligonucleotide (5′-TCGAGCTCGGTACCCGGGGATCCTCTAGA**G**TCGACCTGCAGGCATGCAAGC-3′) to create a G:U mismatch base pair substrate. Apyrimidinic sites were cleaved by basic pH and high temperature (90°C for 3 minutes). The cleaved and uncleaved oligonucleotides were separated on a 15% TBE-urea-acrylamide gel, and bands were quantified by densitometry.

*Ung reverse-transcriptase PCR analysis*. Total RNA was isolated from WT or $Ung^{neo/hygtk}$ ES cells by use of the Qiagen RNeasy kit (Qiagen, Hilden, Germany) as per the manufacturer's protocol. Oligo-(dT) directed cDNA was prepared as follows: 10 μg total RNA and 1 μg oligo-(dT) (Gibco-BRL) were incubated at 75°C for 10 minutes and quick chilled on ice. First-strand cDNA synthesis was then carried out with MuLV reverse-transcriptase (RT) (Superscript II; Gibco-BRL) at 37°C for 60 minutes in the buffer provided by the manufacturer, with the enzyme supplemented by 250 μM of each dNTP. Gene-specific primers are indicated below. PCR amplification was performed in a final volume of 50 μl by utilizing the reaction buffer provided by the manufacturer (PerkinElmer, Wellesley, Massachusetts, USA) supplemented by 200 μM of each dNTP, 20 pmol of each forward and reverse primer, 2 μl of the cDNA reaction mix, and 2.5 units of AmpliTaq Gold DNA polymerase (PerkinElmer). The reaction mixture was subjected to 30 cycles in an MJ Research PT-200 (MJ Research Inc., Waltham, Massachusetts, USA). The denaturation, annealing, and extension conditions were as indicated below for each primer set, followed by a single primer extension step at 72°C for 10 minutes. RT-PCR analyses included the genes that expressed UNG, AAG, TDG, OGG1 AP endonuclease (APE), and actin. Details for the RT-PCR are given in Table 4.

*Northern blots*. Total RNAs were extracted from brain and other tissues by use of a RNAzol kit (Tel-Test, Friendswood, Texas, USA). The products were resolved on an agarose gel, transferred to nylon membrane, and hybridized in Church buffer (0.5 M $NaPO_4$; pH 7.5; 7% SDS; 2 mM EDTA) with a radioactive-labeled probe for 8 to 16 hours at 63°C. Radioactive-labeled probes were synthesized with a random labeling. Final wash was 0.1 × SSC, 0.1% SDS at 62°C. Intensities of hybridized bands were measured by densitometry and normalized to hybridization with β-actin.

*Mutation assays in mouse cells*. A small number of ES cells (<50) were seeded and independently expanded in the absence of mouse embryonic feeder cells to the desired cell number. The expanded final cell population was trypsinized, counted, and plated in medium containing 2 μM of ganciclovir to select for thymidine kinase (TK) mutants. The selection was performed at a density not greater than $10^7$ cells per 150-mm dish in the absence of mouse embryonic feeder cells. Drug-resistant medium was changed frequently. After 14 days of selection, drug-resistant colonies were counted, picked, and further expanded for analysis. All BigBlue *cII* mutation assays were performed as described previously (30). Briefly, genomic DNA was extracted from the cells (5 to 10 × $10^6$ cells per sample) using Recoverase DNA Isolation Kits (Stratagene) and stored at 4°C. λ-LIZ (LacI/Z) shuttle vectors were rescued from genomic DNA with Transpack packaging extract according to the manufacturer's protocol (Stratagene). Plaques with mutations in the *cII* gene were determined essentially as described (30). Mutant frequen-

cies were determined using genomic DNA isolated from at least three separate cell samples. For each DNA sample, plaques were analyzed from at least three packaging reactions to ensure an accurate mutant frequency determination.

*SNP exposure and hypoxia*. Approximately 200,000 *Ung*$^{+/+}$ or *Ung*$^{-/-}$ MEFs were exposed to different conditions of SNP (45 μM to 1.2 mM). After SNP exposure, cells were cultivated for additional 24 hours in normal media with DMEM with 10% FBS. For hypoxia experiments, approximately 200,000 *Ung*$^{+/+}$or *Ung*$^{-/-}$ MEF were placed in a chamber and exposed to a hypoxic condition (<5% $O_2$) for 20 hours, followed by cultivation in normal atmosphere for additional 12 hours. At the end of the respective experiments, the final cell population was trypsinized, stained with trypan blue, and counted for vital cells.

*Reversed-phase HPLC*. DNA was extracted using a Qiagen genomic DNA purification kit (Qiagen) (31). Thirty micrograms of DNA were dissolved in 100 μl P1-buffer (30 mM sodium acetate and 0.1 mM zinc sulfate, pH 5.3) and digested with nuclease P1 (ICN, Eschwege, Germany). Then, nucleotides were subjected to bacterial alkaline phosphatase (Sigma-Aldrich) in AP-buffer (50 mM Tris-HCl and 100 μM EDTA, pH 8.0) at 37°C for 8 hours. The resulting nucleosides were separated by gradient reversed–phase, high-pressure liquid chromatography (HPLC-UV system with a Class-LC10 assembly; Shimadzu, Berlin, Germany). The mobile phase was 20 mM ammonium acetate with 2% (solution A) or 80% (solution B) acetonitrile (pH 4.3; flow rate 2 ml/min). The solid phase was a 4.6 mm × 25 cm Supelcosil LC-18S column plus precolumn filter (Supelco, Bellefonte, Pennsylvania, USA; 5-μm particle size). Each run was 12 minutes total (100% solution A from minutes 1 to 4, 15% solution B from minutes 5 to 8.5, 100% solution B from minutes 8.5 to 9, and 100% solution A from minutes 9 to 12). Nucleosides were detected by their distinct UV absorption maxima on an SPD-M10A UV-detector (Shimadzu), and the area under each peak was converted to a mass equivalent by integrating the respective extinction into a equilibration curve. Standard nucleosides (Sigma-Aldrich) were used for identification and quantification.

*Neuronal cell cultures*. Primary neuronal cultures of cerebral cortex were obtained from mouse embryos (E16 to E18) as described (32, 33). Cortices were dissected, trypsinized, dissociated, and plated in 24-well or 6-well plates precoated with poly-L-lysin (0.5% w/v in PBS) and collagen (0.03% w/v) in a density of 200,000 cells/cm$^2$ (for details see ref. 33). Cultures were kept at 36.5°C and 5% $CO_2$ and were fed, beginning from 4 days in vitro (DIV 4), with cultivating medium (starter medium without glutamate) by replacing half of the medium twice a week. Experiments were performed after DIV 10 to DIV 12.

*Oxygen-glucose deprivation, mitochondrial function, and cell death*. For OGD, the medium was removed from cultures and preserved. Cultures were subjected to OGD for 120 minutes (severe) or 80 minutes (mild) in a balanced salt solution at $PO_2$ < 1 mmHg, followed by replacement of the preserved medium as described previously (33). For control, cells were placed in a balanced salt solution with 20 mM D-glucose for 120 or 80 minutes in normoxic atmosphere with 5% $CO_2$. Staining with fluorescein diacetate (FD) and propodium iodide (PI) was performed for assessment of cell viability (1 μg/ml for 20 minutes at 37°C). Pictures of three randomly chosen high-power fields from different cultures were taken and counted by a naive researcher as viable (FD-positive), dead (PI-positive), or early-stage cell death (double). At various time points (1, 3, 9, and 24 hours), aliquots of the medium were saved for analysis of LDH activity as described (33). MTT assay was performed, which measures the amount of blue formazan produced by viable mitochondria from MTT (Sigma-Aldrich) as described (33). In addition, TMRE (Molecular Probes, Leiden, The Netherlands) was used to assess mitochondrial membrane potential as described (34). After experiments, TMRE was added (100 nM, 40 min) and its mitochondrial uptake was assessed by fluorescence microscopy in the multiwell fluorescence reader, and pictures were taken with a fluorescence microscope and a digital camera.

*Mouse model for focal cerebral ischemia*. All animal experiments were conducted in accordance with institutional and international guidelines and approved by local authorities (#0054/99; Landesamt für Arbeitsschutz, Gesundheitsschutz und technische Sicherheit [LAGetSi], Berlin, Germany). Mice (18 to 23 g) were anesthetized with 1.5% halothane (induction) and maintained on 1.0% halothane in 70% nitrous oxide and 30% oxygen. Regional cerebral blood flow (rCBF) was measured by laser Doppler flowmetry (35). In randomly selected animals, the left femoral artery was cannulated for arterial blood pressure and blood gas determination as described (35). Arterial blood samples (50 μl) were analyzed for pH, $PaO_2$, and $PaCO_2$ on a blood gas/pH analyzer (Corning 178; Ciba-Corning Diagnostics, Medford, Massachusetts, USA). MCAo was induced with a silicone-coated, 8-0 monofilament. Thirty minutes later, the filament was completely withdrawn to allow reperfusion. Core temperature was maintained at approximately 37°C ± 0.5°C during the monitoring period.

*Infarct volumes and neuronal survival.* Seventy-two hours after reperfusion, animals were killed and the brains were snap-frozen in isopentane on dry ice. Lesion areas were quantified with an image analysis system (M4; St. Catharines, Ontario, Canada) on 20 μm-hematoxylin and eosin-stained cryostat sections. Volumes were calculated by summing the volumes of each section directly. NeuN immunocytochemistry was performed on cryostat sections by use of mouse monoclonal anti-NeuN antibodies (1:100; Chemicon, Hofheim, Germany) and diaminobenzidine as chromogene. Only cells with a clear nuclear signal were considered NeuN+ and counted in five randomly selected high-power fields (×400 magnification) within the ischemic striatum at the level of the anterior commissure (bregma 0.14) and expressed as number of NeuN+ cells/mm$^2$.

*Neurological deficits*. Mice were tested for neurological deficits by a naive observer 72 hours after MCAo and rated on a scale from 0 (no observable deficit) to 3 (severe) as described (36).

*Carbon black*. Deeply anesthetized mice were transcardially perfused with carbon black (in an equal volume of 20% gelatin in distilled water). Animals were decapitated and heads stored in 3.7% formaldehyde for 3 hours at 4°C. Brains were carefully removed, and the development of left and right posterior communicating arteries (PComAs) was scored as follows: 0, absent; 1, present but poorly developed (hypoplastic); and 2, well formed. A single PcomA development score was calculated by averaging the left and right scores (13). Anastomoses on the dorsal surface of the brain were localized by tracing the peripheral branches of the anterior and middle cerebral artery as described. Adjacent anastomosis points were connected, and the distance from the midline to the line of anastomoses was measured on photographs taken at coronal planes 2 mm, 4 mm, and 6 mm from the frontal pole (14).

*Preparation of extracts from brain tissue*. Mice underwent 30 minutes of MCAo and reperfusion. Mice without ischemia (control) or with a filament inserted into the carotid artery without further advancing it (sham) were prepared. Cortex and striatum of ischemic and corresponding tissue from the contralateral hemisphere were isolated, homogenized (Wheaton homogenizer) in PBS (Gibco), and put on ice. After two washes with 1 ml PBS (1,000 *g* for 10 minutes at 0°C), samples were incubated in 1 ml hypotonic buffer (10 mM HEPES, pH 7.9, 1.5 mM $MgCl_2$, 10 mM KCl, 0.5 mM disodium-EDTA, 0.1 mM EGTA, 1 mM DTT; all from Sigma-Aldrich) with 5 μl of 50 mM PMSF (Sigma-Aldrich) for 10 minutes on ice. Samples were incubated with 30 μl Igepal CA-630 (Sigma-Aldrich) for 5 minutes, centrifuged at 1,000 *g* for 10 minutes at 0°C, and supernatants containing cytoplasmatic extracts were stored at –80°C. Pellets (washed once with 500 μl hypotonic buffer) were dissolved in 250 μl nuclear extract buffer (20 mM HEPES, pH 7.9; 20% glycerol; 420 mM Nacl; 1.5 mM $MgCl_2$; 0.5 mM disodium-EDTA; and 1 mM DTT). Then, 2.5 μl of 50 mM PMSF, 2.5 μl aprotinin (1 mg/ml), 2.5 μl leupeptin (1 mg/ml), and 2.5 μl pepstatin (1 mg/ml) (all from Sigma-Aldrich) were added, and samples were placed on ice for 30 minutes. Cellular debris was removed by centrifugation (13,000 *g* for 10 minutes), and supernatants that contained nuclear extracts were stored at –80°C. Protein concentrations were determined by use of Bradford solution and adjusted to 1 mg/ml.

*Uracil-DNA glycosylase activity assay (brain extracts)*. A Cy5-labeled uracil–containing oligoI (Cy5-5′-AGTCATGCCATTGGCCACATUGTGTCAGCTAGGATT-3′) and complementary oligoII (5′-CAATCCTAGCTGACACGATGTGGCGAATGGCATGAC-3′) were provided by MWG Co (Ebersberg, Germany). A 37-bp oligoduplex formation was allowed by incubating 1.25 pmol of each oligo (I and II) in TE at 95°C for 1 minute and slowly cooling down at 1°C/min to 4°C in a Hybaid (Heidelberg, Germany) thermocycler. For uracil excision, 2.5 pmol of the oligoduplex was incubated with 10 μl cytoplasmatic or nuclear extract, respectively, in 27.5 μl base excision buffer (1 mM NaCl; 2 mM Tris-HCl, pH 7.5; 0.2 mM $MgCl_2$; and 0.1 mM DTT) for 20 minutes at 37°C in a Trio Thermoblock (Biometra, Göttingen, Germany). Electrophoresis on denaturating 19% polyacrylamide gel (30 ml of 30% Rotiphorese gel [Carl Roth GmbH, Karlsruhe, Germany], 12 ml 5× TBE [54 g Tris; 27.5 g boric acid (Carl Roth GmbH); and 20 ml of 0.5 M EDTA, pH 8.0 (Sigma-Aldrich) per 1 l], 15 g urea, [Carl Roth GmbH]) for 110 minutes allowed strand breakage of former uarcil-containing AP sites, which produced a 20-bp Cy5-containing single-stranded fragment. Occurrence of 20-bp fragments was detected by use of an Alf-sequencing machine (55°C, 1500 V, 60 mA, 30W; Pharmacia Biotech, Erlangen, Germany) and the proportion of 20-bp fragments to 37-bp oligoduplex peaks was calculated in terms of percentage (37).

*Data analysis*. Data are presented as mean ± standard error (SEM). Differences between groups were evaluated by ANOVA followed by Tukey's or Scheffe's test; NeuN+ cell counts were compared using the Mann-Whitney *U* test; neurological sensory-motor deficits scores and PcomA patency scores were analyzed by nonparametric ANOVA on ranks (Kruskal Wallis) followed by Dunn's test. *P* values of less than 0.05 were considered of statistical significance.

## Acknowledgments

We are grateful to J. T. Molina for initiating research on the mouse *Ung* gene in our laboratory. We thank Michael A. Moskowitz for providing laboratory equipment and Dirk Megow for advice. This research was supported by the Deutsche Forschungsgemeinschaft (Heisenberg-Program [M.E.]), the Fritz-Thyssen-Stiftung and Deutscher Akademischer Austausch Dienst (DAAD) (D.B), the University of Pittsburgh Cancer Institute (R.W.S.) and the Hermann and Lilly Schilling Foundation (U.D.).

Received for publication December 29, 2003, and accepted in revised form April 14, 2004.

Address correspondence to: Matthias Endres, Klinik und Poliklinik für Neurologie, Charité-Universitätsmedizin Berlin, Campus Mitte, Schumannstrasse 20/21, D-10117 Berlin, Germany. Phone: 49-30-450-560-020; Fax: 49-30-450-560-932; E-mail: matthias.endres@charite.de.

Matthias Endres and Detlev Biniszkiewicz contributed equally to this work.

1. Krokan, H.E., et al. 2001. Properties and functions of human uracil-DNA glycosylase form the *Ung* gene. *Prog. Nucleic Acids Res.* **68**:366–386.
2. Viswanathan, A., You, H.J., and Doetsch, P.W. 1999. Phenotypic change caused by transcriptional bypass of uracil in nondividing cells. *Science*. **284**:159–162.
3. Glassner, B.J., Rasmussen, L.J., Najarian, M.T., Posnick, L.M., Samson, L.D. 1998. Generation of a strong mutator phenotype in yeast by imbalanced base excision repair. *Proc. Natl. Acad. Sci. U. S. A.* **95**:9997–10002.
4. Krokan, H.E., Nilsen, H., Skorpen, F., Otterlei, M., and Slupphaug, G. 2000. Base excision repair of DNA in mammalian cells. *FEBS Lett.* **476**:73–77.
5. Duncan, B.K., and Weiss, B. 1982. Specific mutator effects of ung (uracil-DNA glycosylase) mutations in *Escherichia coli*. *J. Bacteriol.* **151**:750–775.
6. Impellizzeri, H.E., Anderson, B., and Burgers, P.M. 1991. The spectrum of spontaneous mutations in a *Saccharomyces cerevisiae* uracil-DNA glycosylase mutant limits the function of this enzyme to cytosine deamination repair. *J. Bacteriol.* **173**:6807–6810.
7. Nilsen, H., et al. 2000. Uracil-DNA glycosylase (UNG)-deficient mice reveal a primary role of the enzyme during DNA replication. *Molecular Cell.* **5**:1059–1065.
8. Nilsen, H., et al. 2001. Excision of deaminated cytosine from the vertebrate genome: role of the SMUG1 uracil-DNA glycosylase. *EMBO J.* **20**:4278–4286.
9. Chatterjee, A., and Singh, K.K. 2001. Uracil-DNA glycosylase-deficient yeast exhibit a mitochondrial mutator phenotype. *Nucleic Acids Res.* **29**:4935–4940.
10. Liu, P.K, Grossmann, R.G., Hsu, C.Y., and Robertson, C. 2001. Ischemic injury and faulty gene transcripts in the brain. *Trends Neurosci.* **24**:581–588.
11. Choi, D.W. 1995. Calcium: still center-stage in hypoxic-ishemic neuronal death. *Trends Neurosci.* **18**:58–60.
12. Wink, D.A., et al. 1991. DNA deaminating ability and genotoxicity of nitric oxide and its progenitors. *Science*. **254**:1001–1003.
13. Majid, A., et al. 2000. Differences in vulnerability to permanent focal cerebral ischemia among 3 common mouse strains. *Stroke*. **31**:2707–2714.
14. Maeda, K., Hata, R., and Hossmann, K.-A. 1998. Differences in cerebrovascular anatomy of C57Black/6 and SV129 mice. *NeuroReport*. **9**:1261–1265.
15. Otterlei, M., et al. 1999. Postreplicative base excision repair in replication foci. *EMBO J.* **18**:3834–3844.
16. Neddermann, P., et al. 1996. Cloning and expression of human G/T mismatch-specific thymine-DNA glycosylase. *J. Biol. Chem.* **271**:12767–12774.
17. Hendrich, B., Hardeland, U., Ng, H.-H., Jiricny, J., and Bird, A. 1999. The thymine glycosylases MBD4 can bind to the product of deamination at methylated CpG sites. *Nature*. **401**:301–304.
18. Green, D.R., and Reed, C.J. 1998. Mitochondria and apoptosis. *Science*. **281**:1309–1312.
19. Green, D.R., and Kroemer, G. 1998. The central executioners of apoptosis: caspases or mitochondria? *Trends Cell. Biol.* **8**:267–271.
20. Chen, D., et al. 2003. Upregulation of mitochondrial base-excision repair capability within rat brain after brief ischemia. *J. Cereb. Blood Flow Metab.* **23**:88–98.
21. Pinz, K.G., and Bogenhagen, D.F. 1998. Efficient repair of basic sites in DNA by mitochondrial enzymes. *Mol. Cell. Biol.* **18**:1257–1265.
22. Chen, D., Lan, J., Pei, W., and Chen, J. 2000. Detection of DNA base-excision repair activity for oxidative lesions in adult brain mitochondria. *J. Neurosci. Res.* **61**:225–236.
23. Chen, D., et al. 2002. Age-dependent decline of DNA repair activity of oxidative lesions in rat brain mitochondria. *J. Neurochem.* **81**:1273–1284.
24. Croteau, D.L., Stierum, R.H., and Bohr, V.A. 1999. Mitochondrial DNA repair pathways. *Mutat. Res.* **434**:137–148.
25. Endres, M., et al. 1998. Attenuation of delayed

neuronal cell death after mild focal ischemia by inhibitors of the caspase family. *J. Cereb. Blood Flow Metab.* **18**:238–247.
26. Keyvani, K., Witte, O.W., and Paulus, W. 2002. Gene expression profiling in perilesional and contralateral areas after ischemia in rat brain. *J. Cereb. Blood Flow Metab.* **22**:153–160.
27. Schneider, A., et al. 2004. Restriction-mediated differential display (RMDD) identifies pip92 as a pro-apoptotic gene product induced during focal cerebral ischemia. *J. Cereb. Blood Flow Metab.* **24**:224–236.
28. Li, Z.W., et al. 1996. Generation of mice with a 200-kb amyloid precursor protein gene deletion by Cre recombinase-mediated site-specific recombination in embryonic stem cells. *Proc. Natl. Acad. Sci. U. S. A.* **93**:6158–6162.
29. Li, M., and Bernard, O. 1992. FDC-P1 myeloid cells engineered to express fibroblast growth factor receptor 1 proliferate and differentiate in the presence of fibroblast growth factor and heparin. *Proc. Natl. Acad. Sci. U. S. A.* **89**:3315–3319.
30. Sobol, R. W., et al. 2002. Mutations associated with base excision repair deficiency and methylation-induced genotoxic stress. *Proc. Natl. Acad. Sci. U. S. A.* **99**:6860–6865.
31. Liu, P.K., et al. 1996. Damage, repair and mutagenesis in nuclear genes after mouse forebrain ischemia-reperfusion. *J. Neurosci.* **16**:6795–6806.
32. Brewer, G.J. 1995. Serum-free B27/neurobasal medium supports differentiated growth of neurons from the striatum, substantia nigra, septum, cerebral cortex, cerebellum, and dentate gyrus. *J. Neurosci. Res.* **42**:674–683.
33. Harms, C., et al. 2001. Melatonin is protective in necrotic but not in caspase-dependent, free-radical-independent apoptotic neuronal cell death in primary neuronal cultures. *FASEB J.* **14**:1814–1824.
34. Heiskanen, K.M., Bhat, M.B., Wang, H.W., and Ma, J. 1982. Mitochondrial depolarization accompanies cytochrome *c* release during apoptosis in PC6 cells. *J. Biol. Chem.* **274**:2654–2659.
35. Endres, M., et al. 1998. Stroke protection by 3-hydroxy methylglutaryl-CoA reductase inhibitors mediated by endothelial nitric oxide synthase. *Proc. Natl. Acad. Sci. U. S. A.* **95**:8880–8885.
36. Endres, M., Wang, Z.-Q., Namura, S., Waeber, C., and Moskowitz, M.A. 1997. Ischemic bran injury is mediated by the activation of poly(ADP-ribose) polymerase. *J. Cereb. Blood Flow Metab.* **17**:1143–1151.
37. Engelward, B.P., et al. 1997. Base excision repair deficient mice lacking the Aag alkyladenine DNA glycosylase. *Proc. Natl. Acad. Sci. U. S. A.* **94**:13087–13092.